Desalination and Water Treatment
www.deswater.com

doi:10.5004/dwt.2018.22449

116 (2018) 129–136
June

Removal of ferrous from the wastewater with high-concentration heavy metal by induced crystallization

Wei Song[a], Caixia Fu[b], Ji Li[a,*], Xiaolei Zhang[a]

[a]*School of Civil and Environmental Engineering, Shenzhen Key Laboratory of Water Resource Application and Environmental Pollution Control, Harbin Institute of Technology Shenzhen Graduate School, Shenzhen 518055, China, Tel. +86 15889433623, email: songwei@stmail.hitsz.edu.cn (W. Song), Tel. +86 15889433623, Fax +86-755-26703651, email: liji99@gmail.com, liji98@tsinghua.org.cn (J. Li), Tel. +86 13544185335, email: xiaolei.zhang2016@foxmail.com (X. Zhang)*
[b]*School of Environmental Science and Engineering, Shenzhen Key Laboratory of Soil and Groundwater Pollution Control, South University of Science and Technology of China, Shenzhen 518055, Tel. +86 13715359653, email: fucx@mail.sustc.edu.cn (C. Fu)*

Received 9 September 2017; Accepted 4 May 2018

ABSTRACT

This work had proposed an effective solution to treat the iron-containing heavy metal wastewater by induced crystallization. In this study, a hydraulic fluidized-bed reactor was employed to remove ferrous from the high-concentration heavy metal wastewater. Sand grains (Fe free) were used as carriers. It was found that the optimum initial pH, molar ratio of $[CO_3^{2-}]/[Fe^{2+}]$, HRT and the hydraulic loading were 3.0–3.5, 2.0:1, 40 min and 31 m/h, respectively. Under the optimal condition, Fe^{2+} removal rate reached above 95% when the initial concentration was 100 mg/L. The average particle diameter of the carriers increased from 0.32 mm to 0.48 mm during the continuous operation for 30 days. In addition, crystalline products were observed on the surface of the sand grains and Fe was detected in the products. The study revealed that hydraulic fluidized-bed reactor had great potential on removal from the wastewater containing high-concentration heavy metal.

Keywords: Ferrous removal; Crystallization; Fluidized-bed reactor; Wastewater

1. Introduction

Heavy metals are widely utilized in the industrial process such as metal plating, electric, smelting, alloy casting, and etc. [1,2]. The wastewater generated from the industries normally contains a high concentration of heavy metals. This type of wastewater is categorized as high-concentration heavy metal wastewater. In addition, various heavy metal wastewater may also contain plenty of iron which has two different valence states in nature. The iron could be produced in the different stages of the metal processing and manufacturing industries, such as mining, metal-containing hazardous waste treating, metal etching and electroplating. In addition, heavy metal wastewater after being treated with Fenton reagent also contains large amounts of iron [3].

With the rapid development of industrialization, the quantity of wastewater containing high-concentration heavy metal is gradually increasing. The non-biodegradable and persistent are a great concern because it could cause the environmental-cancer-in the long-term accumulation and global circulation [4,5]. Thus, the drastic increasing of the heavy metal wastewater and the potentially carcinogenic risk to humans have been drawn more attention to the removal and recovery of the heavy metal [6,7].

When treating iron-containing heavy metal wastewater,the traditional physic-chemical methods presented various problems. The precipitate of hydroxides [8] or sulfides [9] were classified as hazardous waste which required complex and expensive treatment [10]. The other methods, including ion exchange [11], red ox process [12] and membrane separation [13–15], required a complex operation and high cost.

*Corresponding author.

1944-3994 / 1944-3986 © 2018 Desalination Publications. All rights reserved.

As the induced crystallization process was proved to remove several heavy metals effectively and without large amount sludge production [11,16–18], the ferric-containing wastewater would lead to the completely different effect according to the practical application to the treatment of electroplating wastewater. However, when to solve the contradiction between the influence of ferric and the advantage of the induced crystallization, the change of the ferric should be considered. As the most widely existed metal, iron had two different valence states in nature normally co-existed with other heavy metals. Since the tri-valence state could not be removed by induced crystallization and also interfered with the treatment of other metals, the bi-valence state may have the positive effect during the induced crystallization. Therefore, it is necessary to identify the result and process of ferrous removed by induced crystallization.

However, the influence of ferric hasn't been considered into the process of the induced crystallization to remove other metals and the effect of ferrous has not yet been studied during the process. Therefore, researchers were focused on seeking valid solutions to apply the induced crystallization into the treatment of iron-containing heavy metal waste water effectively. In this study, the removal of Fe^{2+} by the induced crystallization process in a hydraulic-fluidized-bed reactor (HFBR) was explored. The operating parameters, including the initial pH, the molar ratio of $[CO_3^{2-}]/[Fe^{2+}]$, HRT and the hydraulic loading were optimized. Scanning Electron Microscope (SEM), Energy Dispersive X-Ray Spectroscopy (EDX) and Malvern spray analyzer, were employed to reveal the variation of the surface configuration and demonstrate the crystallization of ferrous.

2. Materials and methods

2.1. Materials

The stock solution of ferrous and precipitation reagent were prepared from $FeSO_4 \cdot 7H_2O$ (99.0%, Crystal) and Na_2CO_3 (99.8%), which were the analytical pure grade chemicals. Other solid reagents purchased from the Sinopharm Chemical Reagent Co., Ltd. The liquid reagents utilized in this study including HCl (analytical pure grade) were from Huateng chemical co., LTD. The quartz sand with the average diameter of 0.25 mm was selected as the crystallizing carriers. The chemicals for analysis were prepared by the deionized water (DI).

Peristaltic pumps (BT100-2J Longerpump, China) were employed to charge the synthetic waste water and the precipitating reagent. The micro-vortex pump (DC40C) achieving the refluxing was provided by the ZKSJ. Co. Ltd. China.

2.2. Synthetic wastewater and precipitation reagent

The synthetic ferrous-containing waste water used in this study were prepared by dissolving $FeSO_4 \cdot 7H_2O$ in tap water. The pH would be adjusted to about 3–4 with hydrochloric acid except for considering the effect of pH. Also, the precipitation reagent was prepared by the Na_2CO_3 dissolved by the tap water. The different concentration of the synthetic wastewater and the precipitation reagent were settled according to the demand of the study.

2.3. Experimental set-up

The experiment was conducted in a hydraulic fluidized-bed reactor made of the PMMA (Polymethyl Methacrylate) with total volume of 3.0 Land a height of 83.0 cm. The schematic diagram of HFBR is shown in Fig. 1, which had the two different inner diameter of 5.0 cm and 13.5 cm from the bottom.

HFBR consisted of three sections: supporting zone, crystallization zone, and settling zone. The supporting zone with the height of 10.0 cm was mainly filled by small stones with the average diameter of 5 mm or 10 mm at the bottom of the reactor. The crystallization zone (20.0 cm) was packed with the quartz sands as the crystal seed with size between 0.20 mm and 0.30 mm diameter. About two-thirds of the HFBR volume was the supporting and the crystal area, while the remaining was the settling and effluent area.

The two inlets are arranged in parallel at the bottom one third of the supporting zone to pump the influent and the precipitation reagent separately. In addition, there are two outlets: the effluent and over fall outlet. The effluent outlet is set at the top of the settling zone, and an over flow gate was designed upon it. Besides, the internal reflux is designed in the reactor, which will transport the discharge in the settling zone into the supporting zone via the reflux pump.

2.4. Process description

The influent mode was up-flow, and carriers were kept in a fluidized state by the micro-vortex pump, which also used to dilute the influent to decrease the treating load. The

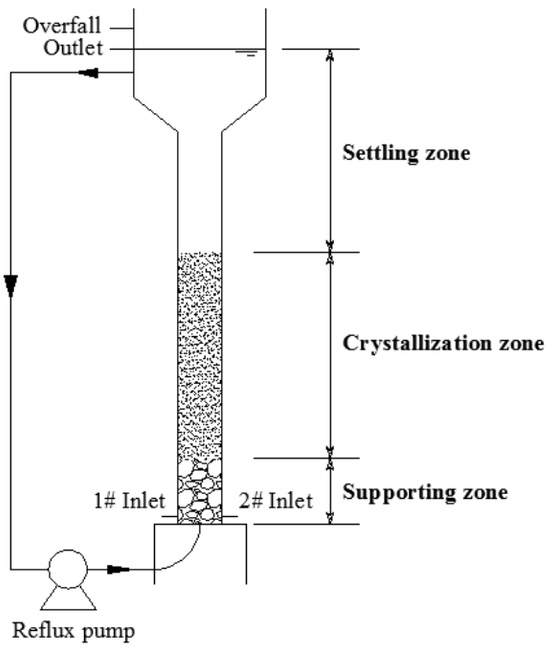

Fig. 1. Diagram of hydraulic fluidized-bed crystallization reactor. The reactor contains three different functional sections: supporting zone, crystallization zone and settling zone. The synthetic wastewater and precipitation will be injected through the 1# inlet and 2# inlet respectively.

synthetic waste water and the precipitating reagents were simultaneously injected into HFBR from separated inlets by the peristaltic pumps. The wastewater was evenly distributed in the crystallization zone as two different particle sizes of quartzes were used in supporting zone. It was expected that the crystallization occurred on the surface of the quartz sands and the crystalline product gradually accumulated at the surface during the process, and hence, ferrous was removed.

2.5. Fe^{2+} induced crystallization

All the experiments were performed at 22~27°C which was the room temperature in the laboratory. Micro-vortex pump was employed to create the fluidized state of the carriers throughout the operation. At the beginning of the study, the HFBR filled with the tap water up to the outlet to make the carriers fluidized after booting there flux system. Thereafter, the synthetic wastewater and the sodium carbonate solution were injected into HFBR from the separated inlets by the peristaltic pumps. The reflux flow rate was adapted by a ball valve made from Teflon and a rotameter was used to measure the flow. During the operation, the molar ratio of $[CO_3^{2-}]/[Fe^{2+}]$ was adjusted to be around 2:1 and the pH of the solution containing $Fe^{2+}$was guaranteed around pH 3.0–3.5, which was adjusted by the hydro chloric acid.

2.6. Sampling and analytical methods

During the crystallization, the ferrous in the influent would convert to three sections: the metal on the surface of the sand, the metal in the suspended solids and the dissolved in the effluent.

The quantitative relation could be expressed as Eq. (1) and Eq. (2).

$$C_{in} = C_{Hete} + C_{out,\,Tot} \tag{1}$$

$$C_{out,Tot} = C_{Hom} + C_{out,\,Diss} \tag{2}$$

where C_{in} is the concentration of iron at the inlet of the reactor, C_{Hete} is the adherent metal heterogeneous crystallized upon the sands carrier, C_{Hom} is the suspended metal homogeneous nucleated in the effluent, $C_{out,Tot}$ is the total concentration of iron at the outlet including the liquid and the solid state, and $C_{out,Diss}$ is the concentration of the dissolved iron at the outlet of the reactor.

Thus, crystallization capacity, η, could be expressed as shown in Eq. (3). The homogeneous nucleation percentage, *W*, could be described as shown in Eq. (4).

$$\eta = (C_{in} - C_{out,Tot})/C_{in} \times 100\% \tag{3}$$

$$W = (C_{out,Tot} - C_{out,Diss})/C_{in} \times 100\% \tag{4}$$

The two indicators, *W* and η, represented the contents and difference between the homogeneous and the heterogeneous nucleation phenomena, respectively.

To track the ferrous during the process, samples (50 mL) were collected from the outlet of the HFBR at the specific time. In addition, the pH and turbidity were measured as well. The pH of the samples was measured with the microprocessor-based pH/ORP Bench Meter (HI2210 HANNA Instruments Co., Ltd.,Italy), which was calibrated before being used in the experiments. The turbidity was determined with a portable turbid meter (DR900 HACH, America).

Ferrous concentration in the effluent was measured based on the Chinese national standard analytical method titled as O-phenanthroline spectrophotometric method using the UV-Vis spectrophotometer (U-1800 Hitachi, Japan) after filtered by the 0.45 μm micro porous filter-aquo system. Ferrous and the total iron were measured. The ferrous in the suspended solids in the effluent was measured with the similar method after treated with moderate hydro chloric acid to dissolve the ferrous in the precipitates and filtration to remove the residual solids.

Crystallization was expected to occur on the surface of the carriers. In order to observe the surface characteristic of the carrier, the scanning electron microscope (SEM, SU-70 Hitachi, Japan) was employed. And the energy dispersive X-ray spectroscopy (EDX, NordlysMax3 Oxford Instruments, UK) was used to analyze the elements of the crystalline. The samples were withdrawn from the reactor before and after crystallization for 30 d, and then washing it by the deionized water three times. The air dried samples were then analyzed with SEM and EDX. The X-ray diffractomer (XRD, D/max-2500/PCRigaku, Japan) and the laser particle size analyzer (Master sizer 2000 Malvern,UK) were used to analyze the phase composition and the particle size distribution of the crystallized product, respectively. The analysis was in triplicates, and the results were the mean values.

3. Results and discussion

3.1. Optimization of operating conditions in ferrous crystallization

3.1.1. Effect of initial pH on ferrous crystallization

The initial pH was an important factor as proper pH could promote the crystallization process just as the opinion that the pH changes could influence the mechanism and the physico chemical characteristics of the crystalline products [19]. Similar description was reported about the importance of pH to the crystallization [20]. Five different pH, including 1.50, 2.00, 3.00, 3.50 and 4.00 were investigated. The initial Fe^{2+} concentration was 100 mg/L with the $[CO_3^{2-}]/[Fe^{2+}]$ of 2:1 and the hydraulic loading of 30 m/h. The relationship between removal efficiency, η and *W*, and the pH of the effluent are shown in Fig. 2.

It was seen that the concentration of the ferrous ion in the effluent was about 40 mg/L when the pH was below 2.0 (Fig. 2) and only half of ferrous could be removed. It could be due to the fact that the high concentration of hydrogen ion would dissolve the crystal substance crystallized upon the carrier surface. When the pH exceeded 4.00, the Fe^{2+} would be oxidized to Fe^{3+} rapidly and then formed into the flocculent precipitation. When the pH was around 3.0, the highest removal efficiency (about 90%) occurred, which reached above 90%. Moreover, the content of the homogeneous precipitation was below 5%. It indicates that the production of the heavy metal could be controlled at the lowest

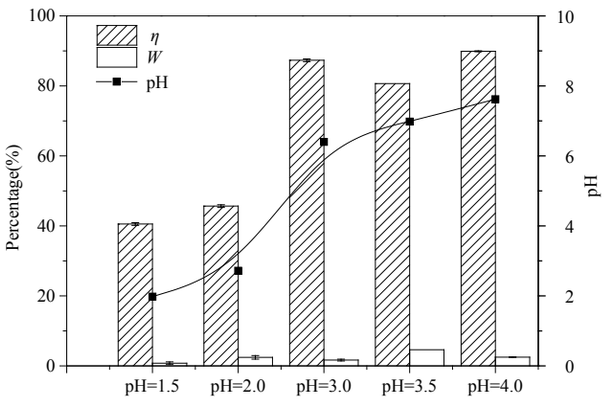

Fig. 2. Effect of Fe^{2+} crystallization under different pH. 100 mg/L influent Fe^{2+}. Molar ratio of $[CO_3^{2-}]/[Fe^{2+}]$ = 2:1. HRT = 40 min and 30 m/h hydraulic loading.

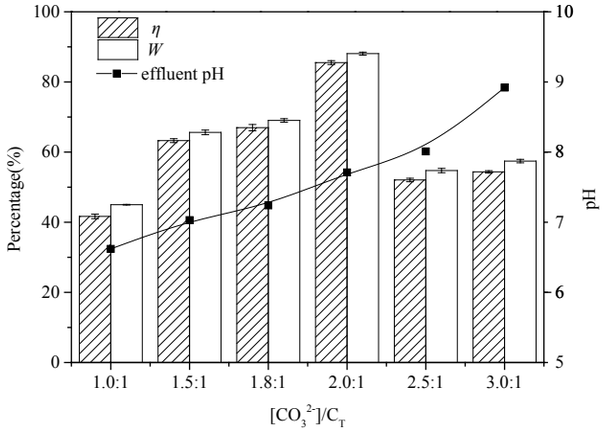

Fig. 3. Effect of Fe^{2+} crystallization under different $[CO_3^{2-}]/[Fe^{2+}]$ value and 100mg/L influent Fe^{2+}, initial pH = 3.5, HRT = 40 min and 30 m/h hydraulic loading.

level when the pH was around 3.0. Generally speaking, the optimal value of the pH could be ranged from 3.0 to 3.5.

3.1.2. Effect of the molar ratio of $[CO_3^{2-}]/[Fe^{2+}]$ on ferrous crystallization

The precipitating reagent, carbonate, was considered as one of the most important factors in the induced crystallization as it could affect the saturability of the function system. Many previous reports raised the importance of the saturation in terms of the nucleation [21,22]. The dosage of sodium carbonate could determine the manner of the nucleating. Not only the supersaturation state was the basis of the crystalline but also the saturability would impel the crystallization. When the crystalline was mixed with other solid impurities, the ideal heterogeneous crystallization would be presented. As to the induced crystallization, the theoretical molar ratio of $[CO_3^{2-}]/[Fe^{2+}]$ was 1:1 as in Eq. (5):

$$Fe^{2+}(aq) + CO_3^{2-}(aq) \rightarrow FeCO_3\,(s) \quad (5)$$

Though the excess Na_2CO_3 solution could ensure the maximum precipitation of ferrous, it might increase the treatment costs. To achieve the best precipitation and utilization of the least dosage, the molar ratio of ($[CO_3^{2-}]/[Fe^{2+}]$) should be investigated.

The molar ratio of $[CO_3^{2-}]/[Fe^{2+}]$, 1.0:1, 1.5:1 and 2.0:1 with the initial Fe^{2+} concentration of 100 mg/L were studied to investigate its impact on ferrous crystallization, respectively. The pH of the influent was controlled at around 3.5 and the hydraulic loading and the HRT was set at 30 m/h and 40 min respectively according to the practical and investigated results. The different results of the corresponding running state, the heterogeneous percentage, the precipitating rate and the effluent pH are shown in Fig. 3.

When the molar ratio of $[CO_3^{2-}]/[Fe^{2+}]$ was 2.0:1, the rate of the heterogeneous crystallization was in the highest level. According to the results (Fig. 3), there was less than 60% of the Fe^{2+} crystallized when the molar ratio of the carbonate, and the ferrous ion was below 2:1. It would be due to the low dosage of carbonate which leads to the lack of contacting opportunity between the precipitator and the ferrous ion. Moreover, when the ratio was higher than the optimal value, the crystallization might also be inhibited due to the exorbitant super saturability. As a previous study described, the metal could not be precipitated completely under the lower molar ratio of $[CO_3^{2-}]/[Fe^{2+}]$. On the contrary, too much CO_3^{2-} present in the reactor that would accelerate the precipitation of discrete precipitates before coating the surface of the carrier to form the nucleated precipitate [23]. Research of silver removal by the induced crystallization revealed the most appropriate feeding ratio of $[CO_3^{2-}]/[Ag^+]$ was 3 mol/mol. It could achieve the most economical dosage of precipitation agent and the sufficient driving force [24].

3.1.3. Effect of HRT on ferrous crystallization

The hydraulic retention time of the reactor had been studied to explore whether it would influence the ferrous crystallization. Choosing the proper retention time could effectively decrease the influent loading and reduce the super saturability of the system, and hence to control the quantity of the homogeneous crystallization. To study the influence of HRT, HRT were varied from 10 min to 60 min. During the operation, the influent concentration of Fe^{2+} and the molar ratio of $[CO_3^{2-}]/[Fe^{2+}]$ were fixed at 100 mg/L and 2:1, respectively. The initial pH of the influent was maintained around 3.00. The result is exhibited in Fig. 4.

It was revealed that the value of η was around 20% and the total removal ratio of Fe^{2+} was less than 40% when the HRT was less than 10 min. However, with the increase of HRT to be longer than 10 min, the crystallization ratio went up to 60%. It showed that more than 80% of the ferrous could be removed through the crystallization at HRT of 40 min (Fig. 4). With short HRT (10, 20, and 30 min), lower ferrous removal rate would be appeared due to the in adequate contact between the metal cation and the carbonate when the HRT was short. However, the longer HRT (50 and 60 min) might have no remarkable effect of the crystallization compared with the HRT of 40 min. A research of the struvite crystalline had indicated that the

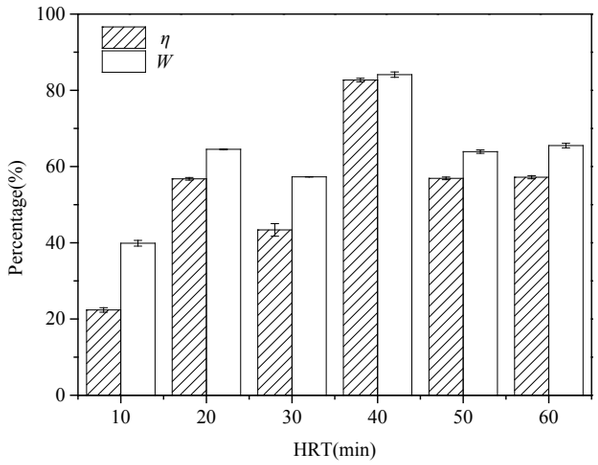

Fig. 4. Effect of Fe^{2+} crystallization under different HRT value and initial pH = 3.5 and 100 mg/L influent Fe^{2+}, molar ratio of $[CO_3^{2-}]/[Fe^{2+}]$ = 2:1 and 30 m/h hydraulic loading.

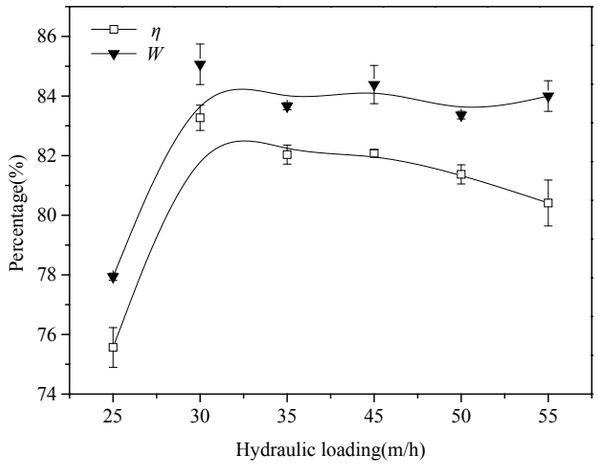

Fig. 5. Effect of Fe^{2+} crystallization under different hydraulic loading value. 100 mg/L influent Fe^{2+} and initial pH = 3.5, molar ratio of $[CO_3^{2-}]/[Fe^{2+}]$ = 2:1 and HRT = 40 min.

HRT also had no prominent influence on the crystallization and it might affect the form or particle size of the crystal [25]. Thus, the optimal HRT was 40 min for ferrous crystallization at the given condition to obtain the highest treating capacity.

3.1.4. Effect of hydraulic loading on ferrous crystallization

When the crystal nucleus penetrated into the interface layer between the crystal and the solution by diffusion, the crystallization would be appeared. The relative speed of turbulence between the solutions and the carriers had the impact on the thickness of the phase interface layer. In the system of crystallization, the reflux could make the carriers absolutely fluidized to realize the phase exchange at the surface of the carriers. Furthermore, the different reflux ratio could realize the variation of the hydraulic loading. Therefore, the hydraulic loading was another important factor in terms of the induced crystallization.

To explore the effect of hydraulic loading in the system, the concentration of ferrous and the pH of the influent was kept at about 100 mg/L and around 3.0, respectively. In addition, the retention time of the reactor was kept at around 40 min. The results are displayed in Fig. 5. It was found that the optimal hydraulic loading was around 31 m/h, which corresponded to the internal reflux ratio of 14~15:1. The loading should not be too low, otherwise it could lead to the insignificant fluidization state and poor contact. On the contrary, the high loading tended to increase the friction among the carriers to wash out the crystallized product. A previous study by Chen on the lead removal from the fluidized-bed reactor also argued the effect of the different hydraulic loading and optimized the proper value [26].

3.1.5. Effect of different concentration of Fe^{2+} on ferrous crystallization

The influent concentration of the ferrous also could impact on the crystallization. The higher concentration

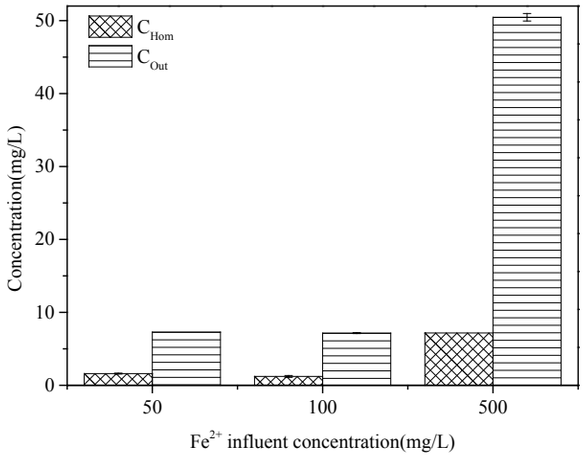

Fig. 6. Effect of Fe^{2+} crystallization under different Fe^{2+} concentration value. Initial pH = 3.5 and the molar ratio of $[CO_3^{2-}]/[Fe^{2+}]$ = 2:1. HRT = 40 min and 30 m/h hydraulic loading.

could increase the supersaturability in the inlet region which could make it different between the whole and the part of the reactor. Exactly, the different supersaturability between the two controlled the nucleation mode.

Three concentrations of ferrous, including 50 mg/L, 100 mg/L and 500 mg/L were used to reflect the different level of influent loading. The other parameters, including pH, HRT, and the molar ratio of $[CO_3^{2-}]/[Fe^{2+}]$ were controlled in the optimal level so that these factors would not disturb the study of the effect of influent concentration. The total concentration of Fe and the content of the homogeneous crystallization were analyzed and are shown in Fig. 6.

It revealed that the crystallization ratio could also be above 90% regardless of the influent concentration. It indicates that the nucleation could occur in this three concentration of ferrous. The results were consistent with the study by de Luna [17].

3.2. Properties of the crystallization products

In the induced crystallization process, the metal ions will react with the special precipitation agent to form the crystalline precipitate. Once there are several heterogeneous carriers, the crystalline will grow upon the surface of the carriers because of reduction of nucleation energy [27].

3.2.1. SEM and EDX analysis of the surface of the carrier

The samples for SEM analysis were prepared by the suitable procedures described above. The SEM was employed to analyze the surface of the carrier to ascertain whether the product could really grow upon the surface of the carriers qualitatively. The images of fresh carrier and used carrier (sampled after two-day operation) from SEM are shown in Figs. 7a and 7b, respectively.

It showed that there was significant difference between the fresh and the used carrier of the morphology. The obvious sharpness structures were observed in the fresh carrier, and it was much smoother than the used carrier. As a contrast, there were plenty of crystal sediments, which had parceled the whole particle, but it had no stationary form because of the blended crystallization. The result demonstrated that the removal of ferrous in the reactor was attributed to its crystallization at the surface of the carriers, and it was consistent with the research conducted by other researchers [21,28].

Then the overall perspective of the carriers during the process was investigated by SEM as well to certify that the

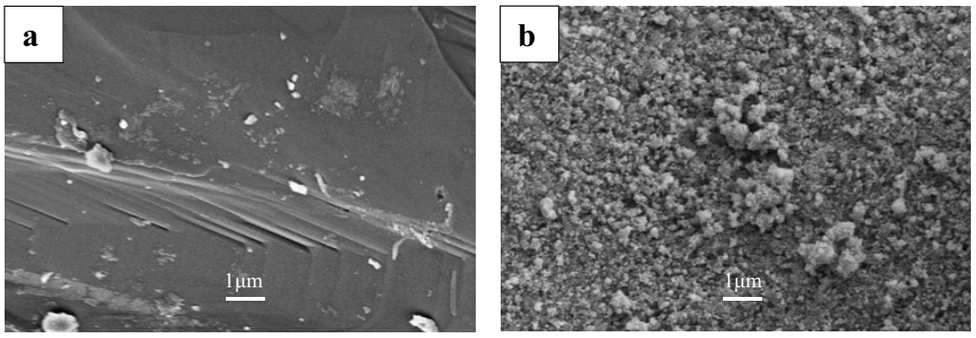

Fig. 7. SEM images of (a) the fresh carrier and (b) crystallized carrier for 2 d. The crystallization parameters: the initial pH = 3.5 and 100 mg/L influent Fe^{2+}, HRT = 40 min and the molar ratio of $[CO_3^{2-}]/[Fe^{2+}]$ = 2:1.

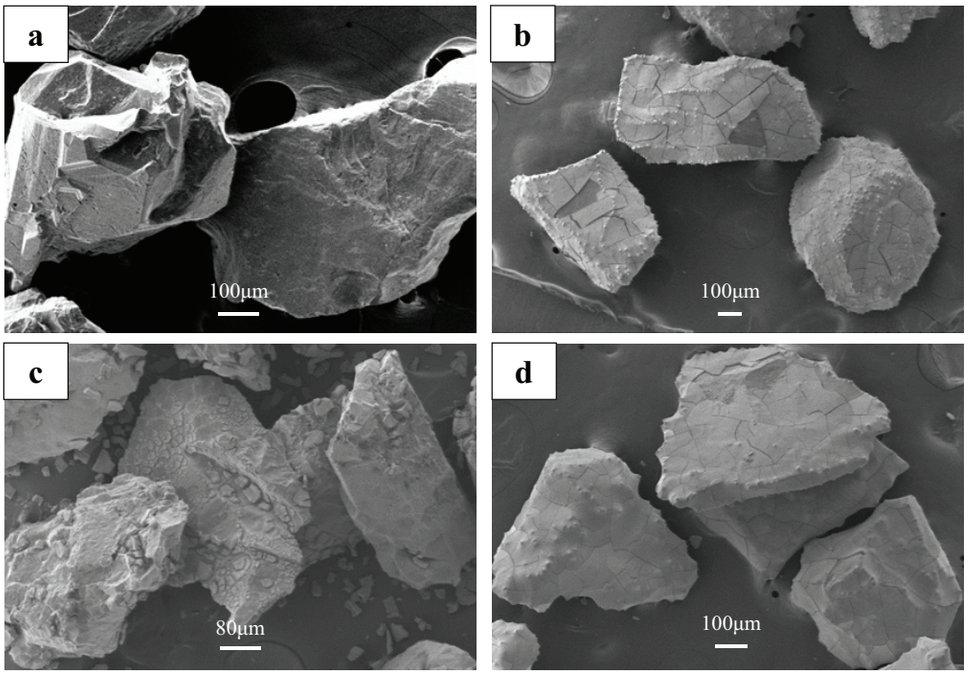

Fig. 8. The SEM images of the growth process of Fe^{2+} crystallization particle. (a) the initial carrier, (b) the carrier crystallized for 5 d, (c) the carrier crystallized for 10 d, (d) the carrier crystallized for 30 d. The crystallization parameters: the initial pH = 3.5 and 100 mg/L influent Fe^{2+}, HRT = 40 min and the molar ratio of $[CO_3^{2-}]/[Fe^{2+}]$ = 2:1.

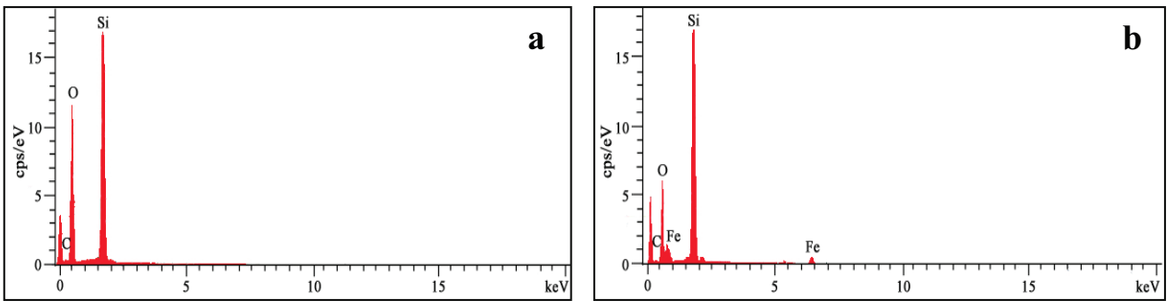

Fig. 9. EDX picture of (a) the fresh carrier and (b) crystallized carrier for 2 days. The crystallization parameters: the initial pH = 3.5 and 100 mg/L influent Fe^{2+}, HRT = 40 min and the molar ratio of $[CO_3^{2-}]/[Fe^{2+}]$ = 2:1.

crystallization occurred throughout the reactor quickly and steadily. The samples were selected from the reactor at the pre-set elapsed time. Fig. 8 shows the apparent change during the continuous operation. The sharp structures were gradually softened by the crystal product. Fig. 8c emerges serious fragmentation phenomena. The operating malfunction led to the crush of the crystal product, and it could revegetate along with the sustained operation as shown in Fig. 8d.

The crystallization process could be further proved by the analysis result of the elemental composition. To detect the elemental composition and estimate the change of the carrier surface, EDX was used to analyze the fresh and used carrier. The different energy spectrums are shown in Figs. 9a and 9b. According to the analysis, it was found that the fresh carrier contained the elements of carbon, oxygen and silicon; however, the iron was detected at the surface of the used carrier. It indicated that the ferrous crystalline had wrapped around the grain sands.

3.2.2. The particle size distribution of crystal granular

The obvious growth of crystal product on the carriers was confirmed by the analysis. In fact, there was another method to verify the crystallization process which was to analyze the particle size distribution among the different crystal stage. In the study, the practical particle sizes of the aforementioned four samples (initial, after five-day operation, after 10-day operation, after 30-day operation) were analyzed. Fig. 10 reveals different particle size distributions, and it expresses the quantity percentage of various particle sizes in the samples.

It was easy to find out that the mean diameter of the granular had increased from 0.32 mm to 0.48 mm during the continuous crystallization process for 30 d. Because of the steady growth of the carriers, the average diameter of the particle gradually increased and caused the shifting of the peak point which represented the distribution on the particle size.

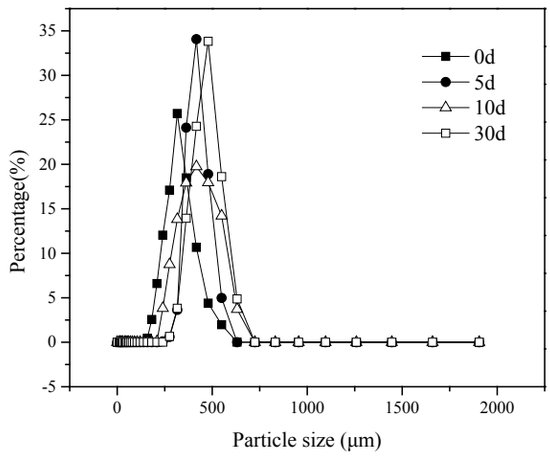

Fig. 10. Particle size distribution curves of Fe^{2+} crystallization. The crystallization parameters: the initial pH = 3.5 and 100 mg/L influent Fe^{2+}, HRT = 40 min and the molar ratio of $[CO_3^{2-}]/[Fe^{2+}]$ = 2:1.

4. Conclusions

When we had transformed the iron into the bi-valence state of the iron-containing heavy metal wastewater, all the metal could be removed effectively by induced crystallization. It was visible for removing the ferrous from the wastewater based on the technology inducing nucleated precipitation of Fe^{2+} on the surface of the sand grains. Under the optimum conditions, ferrous removal efficiency could achieve above 95% when the influent concentration was 100 mg/L.

There were many visible crystalline precipitates without permanent morphology grown over the surface of the carriers according to the SEM images. The elementary composition in the product contained Fe compared with the fresh carrier in terms of the EDX analysis. The average particle diameter varied from 0.32 mm to 0.48 mm during the continuous operation for 30 d. This different detection could verify the removal of Fe^{2+} by the crystallization process.

Acknowledgement

Sincere thanks are to the Major Project of National Water Pollution Control and Governance of Science and Technology (2017ZX07401001), Shenzhen Demonstration Project (KJYY20171012140149523), the National Major Science and Technology program for Water Pollution Control and Treat-

ment (2015ZX07406-004) and the Urban Water Pollution Control and Management Generic Technology Program (2012ZX07206-002).

References

[1] S. Janyasuthiwong, E.R. Rene, G. Esposito, P.N.L. Lens, Effect of pH on Cu, Ni and Zn removal by biogenic sulfide precipitation in an inversed fluidized bed bioreactor, Hydrometallurgy, 158 (2015) 94–100.
[2] M. Gopi Kiran, K. Pakshirajan, G. Das, A new application of anaerobic rotating biological contactor reactor for heavy metal removal under sulfate reducing condition, Chem. Eng. J., 321 (2017) 67–75.
[3] A. Mishra, B.D. Tripathi, A.K. Rai, Enhanced biosorption of metal ions from wastewater by Fenton modified Hydrilla verticillata dried biomass, Int. J. Environ. Sci. Technol., 12 (2015) 3443–3456.
[4] K.M. Al-Qahtani, Water purification using different waste fruit cortexes for the removal of heavy metals, J. Taibah Univ. Sci., 10 (2016) 700–708.
[5] S.R. Smith, A critical review of the bioavailability and impacts of heavy metals in municipal solid waste composts compared to sewage sludge, Environ. Int., 35 (2009) 142–156.
[6] E. European Commission DG, Heavy Metals in Waste, in, Final Report, 2002.
[7] Y. Cai, C. Li, D. Wu, W. Wang, F. Tan, X. Wang, P.K. Wong, X. Qiao, Highly active MgO nanoparticles for simultaneous bacterial inactivation and heavy metal removal from aqueous solution, Chem. Eng. J., 312 (2017) 158–166.
[8] H. Hase, T. Nishiuchi, T. Sato, T. Otake, T. Yaita, T. Kobayashi, T. Yoneda, A novel method for remediation of nickel containing wastewater at neutral conditions, J. Hazard. Mater., 329 (2017) 49–56.
[9] A. Ozverdi, M. Erdem, Cu^{2+}, Cd^{2+} and Pb^{2+} adsorption from aqueous solutions by pyrite and synthetic iron sulphide, J. Hazard. Mater., 137 (2006) 626–632.
[10] M.A. Barakat, New trends in removing heavy metals from industrial wastewater, Arabian J. Chem., 4 (2011) 361–377.
[11] J. Jachuła, Z. Hubicki, Removal of Cr(VI) and As(V) ions from aqueous solutions by polyacrylate and polystyrene anion exchange resins, Appl. Water Sci., 3 (2013) 653–664.
[12] S.S. Chen, C.Y. Cheng, C.W. Li, P.H. Chai, Y.M. Chang, Reduction of chromate from electroplating wastewater from pH 1 to 2 using fluidized zero valent iron process, J. Hazard. Mater., 142 (2007) 362–367.
[13] N. Ghaemi, A new approach to copper ion removal from water by polymeric nanocomposite membrane embedded with γ-alumina nanoparticles, Appl. Surf. Sci., 364 (2016) 221–228.
[14] A. Lee, J.W. Elam, S.B. Darling, Membrane materials for water purification: design, development, and application, Environ. Sci.: Water Res. Technol., 2 (2016) 17–42.
[15] W.W. Li, H.Q. Yu, Z. He, Towards sustainable wastewater treatment by using microbial fuel cells-centered technologies, Energy Environ. Sci., 7 (2013) 911–924.
[16] Y. Chen, R. Fan, D. An, Y. Cheng, H. Tan, Water softening by induced crystallization in fluidized bed, J. Environ. Sci., 50 (2016) 109–116.
[17] M.D.G. de Luna, L.M. Bellotindos, R.N. Asiao, M.C. Lu, Removal and recovery of lead in a fluidized-bed reactor by crystallization process, Hydrometallurgy, 155 (2015) 6–12.
[18] D. Guillard, A.E. Lewis, Nickel carbonate precipitation in a fluidized-bed reactor, Ind. Eng. Chem. Res., 40 (2001) 5564–5569.
[19] N.C. Bouropoulos, P.G. Koutsoukos, Spontaneous precipitation of struvite from aqueous solutions, J. Cryst. Growth, 213 (2000) 381–388.
[20] M.I.H. Bhuiyan, D.S. Mavinic, R.D. Beckie, Nucleation and growth kinetics of struvite in a fluidized bed reactor, J. Cryst. Growth, 310 (2008) 1187–1194.
[21] J. Chung, E. Jeong, J.W. Choi, S.T. Yun, S.K. Maeng, S.W. Hong, Factors affecting crystallization of copper sulfide in fed-batch fluidized bed reactor, Hydrometallurgy, 152 (2015) 107–112.
[22] R. Aldaco, A. Irabien, P. Luis, Fluidized bed reactor for fluoride removal, Chem. Eng. J., 107 (2005) 113–117.
[23] P. Zhou, J.C. Huang, A.W.F. Li, S. Wei, Heavy metal removal from wastewater in fluidized bed reactor, Water Res., 33 (1999) 1918–1924.
[24] D. Wilms, K. Vercaemst, J.C. Vandijk, Recovery of silver by crystallization of silver carbonate in a fluidized-bed reactor, Water Res., 26 (1992) 235–239.
[25] I. Stratful, M.D. Scrimshaw, J.N. Lester, Conditions influencing the precipitation of magnesium ammonium phosphate, Water Res., 35 (2001) 4191–4199.
[26] J.P. Chen, H. Yu, Lead removal from synthetic wastewater by crystallization in a fluidized-bed reactor, J. Environ. Sci. Heal., 35 (2000) 817–835.
[27] W. Stumm, J.J. Morgan, Aquatic Chemistry, 3rd ed., John Wiley & Sons, Inc., New York, 1996.
[28] C.I. Lee, W.F. Yang, C.I. Hsieh, Removal of Cu(II) from aqueous solution in a fluidized-bed reactor, Chemosphere, 57 (2004) 1173–1180.